2024

Aerothermodynamic Analysis of a Linear Aerospike Fueled with Liquid Methane Using CFD

Aidan Rowell
Georgia Southern University

Aerothermodynamic Analysis of a Linear Aerospike Fueled with Liquid Methane Using CFD

An Honors Thesis submitted in partial fulfillment of the requirements for Honors in the Department of Mechanical Engineering

By
Aidan Rowell

Under the mentorship of Dr. Marcel Ilie

ABSTRACT

Renewed interest in manned spaceflight, mostly spurred by the advancement of commercial spacecraft, has led to growing interest in improving the efficiency of rocket engines. Aerospike nozzles have the potential to provide this boost in efficiency to spacecraft and thus lower costs and increase payload capacity. This type of nozzle is what is known as altitude adjusting and can significantly increase efficiency. When paired with propellants such as methane/oxygen, which can be manufactured in-situ on some planetary bodies and has a higher density than traditional propellants like liquid hydrogen/liquid oxygen, even more efficiency gain can be achieved. To understand the capabilities and drawbacks of aerospike nozzles, it is important to model their performance. To this end a comparison of the performance of a linear aerospike fueled with methane/oxygen and hydrogen/oxygen propellants was performed using computational fluid dynamics.

Thesis Mentor: Dr. Marcel Ilie

Honors Dean: Dr. Steven Engel

April 2024
Mechanical Engineering
Honors College
Georgia Southern University

Acknowledgements

I would like to start by expressing gratitude to my mentor for the guidance and support as I have worked on this honors thesis and other projects over the past couple years. I also would like to acknowledge the university and department of mechanical engineering, faculty and staff, as a whole. From those who I have interacted with in class to those I have never spoken to that make sure that the department is running as it should, thank you for all that you do. To those who raised me to be who I am and continue to support me every day, I am eternally grateful. To my friends, current and past, thank you for all your kind encouragement.

Table of Contents

List of Figures

Key Words: Aerospike, Computational Fluid Dynamics, Methane, Propellant

Chapter 1: Introduction

I. Need and Purpose

The rise of commercial launch providers and the introduction of reusable rocket stages like SpaceX's Falcon 9 and Blue Origin's New Shepard Booster stages in the astronautical industry has accelerated the rate at which spacecraft are being deployed into orbit significantly over the past half decade and significantly reduced the cost of payload to low earth orbit (LEO) [1]. On top of this development of next generation fully reusable spacecraft such as SpaceX's Starship are opening the possibility of missions beyond the Earth/Lunar system to places such as Mars.

Success in venturing to places like Mars largely depends on the further reduction of LEO payload costs which as of 2018 sat at a low of around $2,720/kg if using Falcon 9 [1]. This can be done by the incorporation of methods that increase the efficiency of propulsion and utilize resources in the environment to be visited (in-situ). One such method of increasing efficiency is the use of aerospike rocket nozzle geometry as opposed to traditional bell nozzle geometry. This can then be paired with liquid methane fuel, which can be produced in-situ in places such as Mars to lower costs [2-3]. To achieve this, drawbacks of aerospike geometry need to be further investigated.

To understand the implications of using methane in an aerospike, its use in an aerospike engine should be studied. If fueled with methane/oxygen propellant, a lower thrust will be produced due to lower pressure, temperature, and nozzle exit velocity when compared to hydrogen.

Chapter 2: Background and Literature Review

I. Background of Rocket Propulsion

Serious development of the knowledge and theory for rocket propulsion began around the turn of the twentieth century, spearheaded by a few scientists, among which Tsiolkovsky is credited with the creation of the rocket equation (Eq. 1) [4].

$$\Delta v = c_e \cdot ln(\frac{m_0}{m_f}), c_e = I_{sp} g_0 \quad (1)$$

Equation 1 represents a propulsion system's total potential velocity change (often referred to as 'delta v'). The variable c_e is the effective exhaust velocity of the system, m_0 and m_f are the final mass after propellant is exhausted and initial mass of the system, I_{sp} is the specific impulse, and g_0 is gravitational acceleration.

Specific impulse (Eq. 2) is used to describe the efficiency of a rocket propulsion system and is defined as the thrust overweight flow rate [4].

$$I_{sp} = \frac{F}{\dot{m} g_0} = \frac{F}{\dot{w}} \quad (2)$$

The variable F represents the thrust of the propulsion system, $\dot{m}$ represents the mass flow rate of the propellant, and $\dot{w}$ represents the weight flow rate of the propellant.

Thrust is represented by a two-part equation (Eq. 3) divided into a first term (momentum thrust) and a second term (pressure thrust) [4].

$$F = \dot{m} v_2 + (p_2 - p_3) A_2 \quad (3)$$

The variable p_2 represents the pressure at the exit of the nozzle while p_3 represents the ambient pressure and A_2 is the nozzle exit cross sectional area. Rocket engines create thrust by exchanging high temperatures and pressures in their combustion chambers for high exit velocities.

II. Background of Aerospikes

Research into aerospikes (also called plug nozzles) began early on into the 1950s as a possible alternative to traditional bell nozzles. A comparison between the two engine types is shown in Figure 1. Aerospikes are classed as altitude adaptive nozzles, meaning that they exhibit optimum, or close to optimum performance throughout the altitude range of their flight [5-6]. This is highly advantageous as it increases fuel use efficiency, cutting total fuel needs and thus mass, and/or increasing total potential velocity change (Eq. 1).

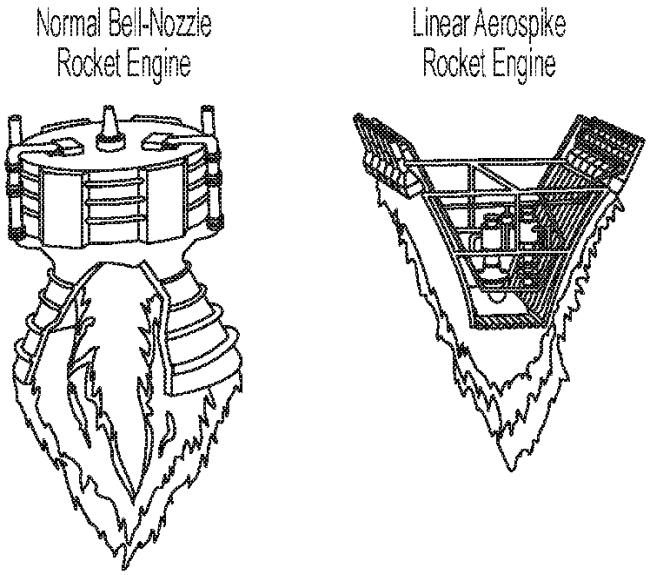

Figure 1. Conventional Bell Nozzle and Linear Aerospike [7].

Aerospike nozzles come in two main configurations: toroidal and linear, the latter being the focus of this paper. For both toroidal and linear aerospikes a design pressure ratio (between the throat of the nozzle and the atmosphere) is chosen, which determines the shape of the spike. At pressure ratios below the design pressure ratio the exhaust flow does not separate from the spike wall and is adapted to changing atmospheric pressure by

recompression shocks and expansion waves emanating from the cowl lip of the nozzle [5-6] (Figure 2). Above the design pressure ratio aerospikes are unable to adjust further, negating their altitude adjustment abilities.

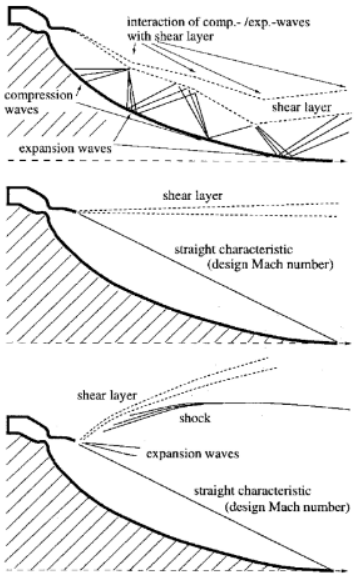

Figure 2. Aerospike Flow at Different Pressure Ratios P_C/P_{atm} [5].

The first tested aerospikes were created by General Electric in 1960, in a range of 16,000 - 50,000 lbs. Thrust [7-8]. During experimentation the aerospikes used for testing were found to be significantly lighter and shorter than conventional nozzles. They were also found to be much less manufacturing and testing intensive when compared to traditional bell nozzles due to their segmented nature [7].

III. Background of Methane/Oxygen Propellant

Use of methane as a fuel has been investigated since the early days of rocket propulsion. Despite this it has only been seriously developed as a fuel in the past two and a half decades. This work has quickly advanced though, with many engines under development or already in use on prototype spacecraft that have yet to go to orbit.

The main benefits of methane are its higher boiling point (111K) as compared to hydrogen (23K), the closeness of its boiling to that of oxygen (90K), its density being six times higher than allowing for smaller fuel tanks, and its ability to be manufactured in-situ [2-3]. Its higher boiling point allows for simplification of the systems involved in storage and engine plumbing, which can reduce the mass of the engine and fuel system overall.

IV. Application

Once performance parameters for an aerospike engine are determined the next step is to define the contour of the throat region and the spike itself. For bell nozzles this has typically been done by using the method of characteristics, originally outlined by G. V. Rao [9]. In this algorithm, characteristic lines that intersect the optimum nozzle contour are defined from the initial conditions present at the throat of the nozzle and the Mach number at the nozzle's exit. This method was then adapted by C.C. Lee [10] and Angelino [11].

Wang et. Al [12] developed a simplified numerical method for design and optimization of aerospike contours that was validated with experimental data. Several linear aerospike configurations were tested. The configuration of interest that will be used as a baseline for simulations is the 3-cell aerospike nozzle with round-to-rectangle primary

nozzles. The parameters used to define the model are shown in Table 1. Thrust reached 3500 N at a chamber pressure of 3.4MPa.

Sullivan [13] developed a CFD model using Ansys Fluent to compare the performance of film cooling and transpiration cooling techniques on an aerospike. A realizable k-ϵ model was used to simulate turbulent viscosity and a species transport model with volumetric reactions was used to model hydrogen oxygen combustion with H_2 having a mass fraction of 0.155 and O_2 having a mass fraction of 0.844, with the remainder being H_2O. Heat transfer was modeled only for convection.

Chapter 3: Methodology

I. Geometry Modeling

To create a useful model a baseline needs to be used to validate any collected data. The geometry used for the conducted simulation was based on physical tests run by Wang et. Al [12], shown in Figure 3, as well as a model based on those physical tests by Sullivan [13].

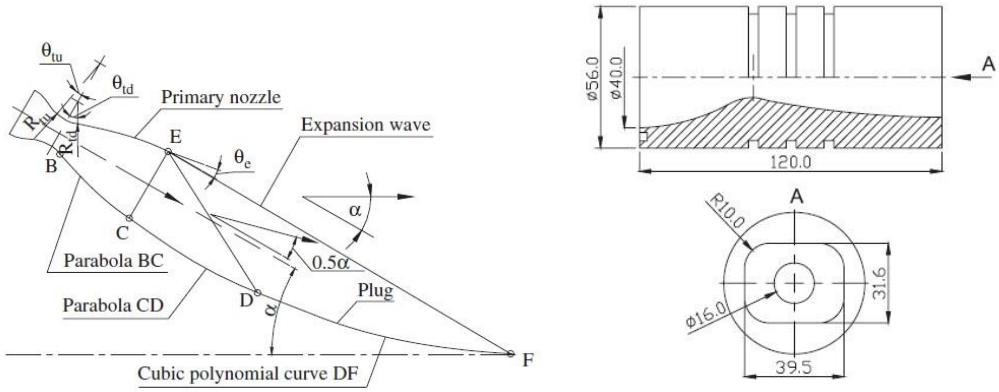

Figure 3. Baseline Geometry Schematic [12].

The geometry consists of a traditional style rocket nozzle with a round-to-rectangle shape, which is followed by a linear aerospike, as shown in Figure 4. Parameters used to derive the geometry are shown in Table 1.

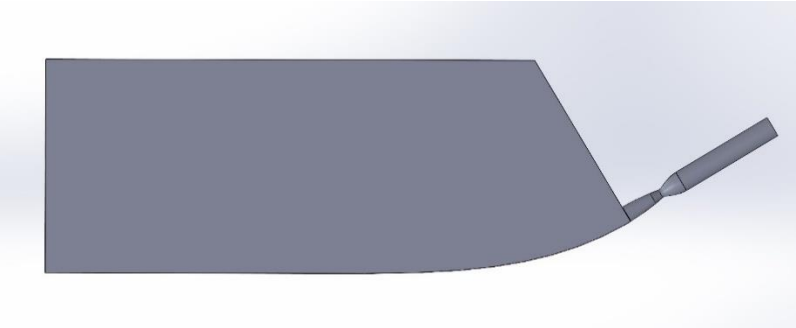

Figure 4. Model Geometry.

Table 1. Parameters for Defining Model [13].

Parameter	**Value**
Mixing Ratio β	5.46
Combustion Chamber Pressure P_C	3.85 [MPA]
Combustion Chamber Temperature T_C	3427 [K]
Specific Heat Ratio γ	1.198
Gas Constant R_g	632.0 [J/kgK]
Total Mass Flow Rate $\dot{m}_{all}$	0.901 [kg/s]
Nozzle Inclination α	37.5°
Overall Area Ratio ε_{all}	80
Round-to-Rectangle Nozzle Area Ratio ε_c	5.77
Nozzle Throat Diameter D_t	16 [mm]
Complete Expansion at NPR	1139

II. Meshing

Meshing was achieved using the ANSYS Fluent meshing tool. This tool allows for a much more streamlined meshing process with better mesh qualities than older meshing tools. A poly-hexcore mesh was used, which was subdivided into zones with different element sizes based on those set by Sullivan [13], shown in Table 2 and Figure 5. This was done using bodies of influence. Subdivision of the mesh allowed for better optimization of element count, which increased resolution in areas of importance like the nozzle throat and aerospike ramp while decreasing resolution in less important areas. The total element count was 788,979.

Table 2. Mesh Zone Sizes [13].

Zone	Element Size
A	8mm
B	4mm
C	2mm
D	3mm

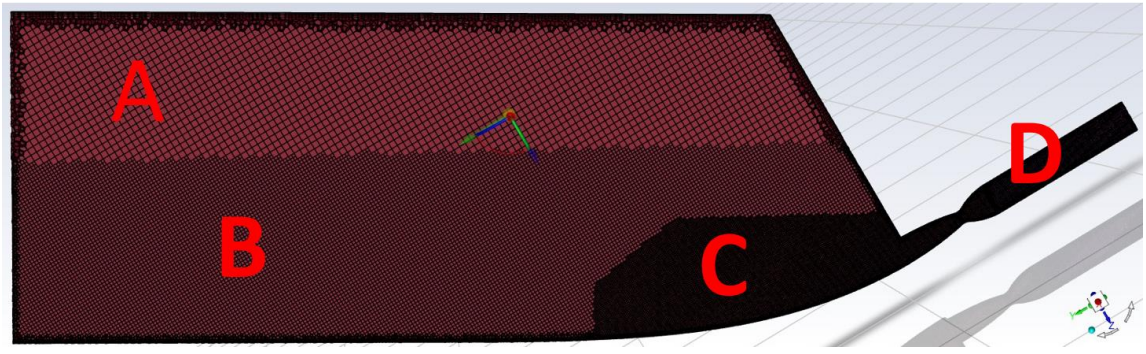

Figure 5. Mesh and Subdivided Zones.

III. Boundary Conditions

The first boundary condition set was a mass flow inlet, shown in Figure 6. It was set to a mass flow rate of 0.300333 kg/s which is 1/3 of the mass flow rate of the three-nozzle ramp used by Wang et al, as the model is restricted to one nozzle for computational reasons [13]. This mass flow rate was used for both the hydrogen/oxygen model and methane/oxygen model. The gauge pressure was set to 0 MPa and the temperature was set to 300K for the hydrogen/oxygen model and 400K for the methane/oxygen model to allow for combustion of the propellant species. For the baseline model a hydrogen oxygen mixture was used and for the experimental model the methane oxygen mixture was used, as shown in Table 3. Experimental model species mass fractions were determined by a molar mass of 20.3 kg/kmol for a methane oxygen mixture [4]. The outlet condition was set to be a pressure outlet, with a gauge pressure of 11,000 Pa, which is the atmospheric pressure determined for the optimum NPR of 1139 [12], and a temperature of 300 K. All species were set to 0 at the pressure outlet. All remaining boundaries were classified as walls, as shown in Figure 6. Propellant species were added to the constant cross-section part of the combustion chamber for each model using ANSYS's patching feature. This was done to ensure a uniform distribution of propellant within the combustion chamber and to prevent the solver from filling the combustion chamber with N_2 by default.

Table 3. Baseline and Experimental Model Species Mass Fraction.

Baseline Model Species	**Species Mass Fraction**
H_2	0.155
O_2	0.844
H_2O	0.001
Experimental Model Species	
CH_4	0.219
O_2	0.779
CO_2	0.001
H_2O	0.001

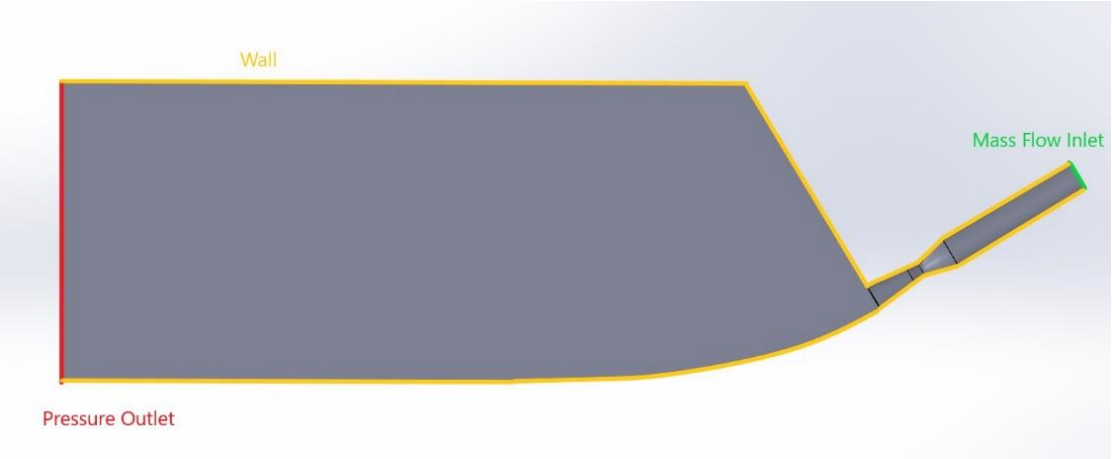

Figure 6. Model Boundary Conditions.

IV. Physics Modeling

To model the processes that take place in the flow a set of specialized equations are used. The model used for turbulence was the realizable k-ε model (Eq. 4-6) [16].

$$\frac{\partial}{\partial t}(\rho k) + \frac{\partial}{\partial x_j}(\rho k u_j) = \frac{\partial}{\partial x_j}\left[\left(\mu + \frac{\mu_t}{\sigma_k}\right)\frac{\partial k}{\partial x_j}\right] + G_k + G_b - \rho\varepsilon - Y_M + S_k \tag{4}$$

and,

$$\frac{\partial}{\partial t}(\rho \varepsilon) + \frac{\partial}{\partial x_j}(\rho \varepsilon u_j) = \frac{\partial}{\partial x_j}\left[\left(\mu + \frac{\mu_t}{\sigma_\varepsilon}\right)\frac{\partial \varepsilon}{\partial x_j}\right] + \rho C_1 S_\varepsilon - \rho C_2 \frac{\varepsilon^2}{k + \sqrt{v\varepsilon}} + C_{1\varepsilon}\frac{\varepsilon}{k} C_{3\varepsilon} G_b + S_\varepsilon \tag{5}$$

where,

$$C_1 = \max\left[0.43, \frac{\eta}{\eta + 5}\right], \eta = S\frac{k}{\varepsilon}, S = \sqrt{2S_{ij}S_{ij}} \tag{6}$$

In the k-ε model the ‘k’ term represents the turbulence kinetic energy and the ‘ε’ term represents the dissipation rate. The realizable k-ε model assumes a fully turbulent flow and includes a modified form of the turbulent viscosity from the standard k-ε model as well as an alternative form of the dissipation rate. As it is realizable, this means that ‘certain mathematical constraints on the Reynolds stresses, consistent with the physics of turbulent flows,’ are satisfied [16]. The term G_k is the generation of turbulence kinetic energy as a result of mean velocity gradients, G_b is the generation of turbulence kinetic energy as a result of buoyancy, Y_M is contributions to the overall dissipation rate due to fluctuating dilation in the compressible turbulence, σ_k and σ_ε are the respective turbulent Prandtl numbers for k and ε, S_k and S_ε are the respective user-defined energy sources, and $C_{1\epsilon}$ and C_2 are constants [16].

Since combustion and heat transfer are being considered the energy equation must be used (Eq. 7).

$$\frac{\partial}{\partial t}(\rho E) + \nabla \cdot \left(\vec{v}(\rho E + p)\right) = \nabla \cdot \left(k_{eff} \nabla T - \sum_j h_j \vec{J_j} + \left(\bar{\bar{\tau}}_{eff} \cdot \vec{v}\right) \right) + S_h \quad (7)$$

In this equation E represents the energy, k_{eff} is the effective conductivity, $\vec{J_j}$ is the diffusion flux of chemical species, and S_h is the source term for volumetric heat sources, including the heat of chemical reactions.

The fluids considered were air and hydrogen-oxygen, labelled hydrogen-air in Fluent, or methane-oxygen, labelled methane-air in Fluent. Each fluid was considered to be an ideal gas (Eq.8). This is because high temperature and low-pressure gases are sufficiently rarified that intermolecular forces and can be considered negligent [17].

$$\rho = \frac{PM}{RT} \quad (8)$$

The viscosity of the reacting mixtures hydrogen/oxygen and methane/oxygen were considered to be constant. At high velocities gases are dominated by inertial forces and viscous forces have a minimal effect, meaning changes in viscosity are minimal and can be considered negligible. The viscosity of air was also modeled as constant.

V. Chemistry Modeling

To account for the chemical species involved in the combustion process the species transport equations with volumetric reactions were used. The species transport equation is

a form of the conservation equation for chemical species in reaction known as a convection-diffusion equation (Eq. 9) [16].

$$\frac{\partial}{\partial t}(\rho Y_i) + \nabla \cdot (\rho \vec{v} Y_i) = -\nabla \cdot \vec{J}_i + R_i + S_i \tag{9}$$

In this equation Y_i is the local mass fraction of the chemical species considered in the problem, R_i is the net rate of species production by chemical reaction, S_i is the rate of species creation from any source determined by the user, and $\vec{J}_i$ is once again the diffusion flux of chemical species, derived from Fick's law [16]. Reactions were carried out with the eddy dissipation model, which accounts for rapid turbulent mixing of species and reaction (Eq. 10-11).

$$R_{i,r} = v'_{i,r} M_{w,i} A \rho \frac{\varepsilon}{k} min\mathcal{R}\left(\frac{Y_{\mathcal{R}}}{v'_{\mathcal{R},r} M_{w,\mathcal{R}}}\right) \tag{10}$$

and

$$R_{i,r} = v'_{i,r} M_{w,i} A B \rho \frac{\varepsilon}{k} \frac{\sum_P Y_P}{\sum_j^N v''_{j,r} M_{w,j}} \tag{11}$$

In these equations, Y_P is the mass fraction of product species, $Y_{\mathcal{R}}$ is the mass fraction of a reactant and A and B are empirical constants with values of 4.0 and 0.5 [16].

The combustion reaction of the baseline hydrogen-oxygen model can be represented by a simple one step reaction (Eq. 12).

$$2H_2 + 2O_2 \rightarrow 2H_2O \tag{12}$$

The combustion reaction for the methane-oxygen model was represented using Fluent's 1-stage reaction mechanism (Eq. 13).

$$2CH_4 + 3O_2 \rightarrow 2CO + 2H_2O \quad (13)$$

Chapter 4: Results and Discussion

I. Baseline Hydrogen Comparison

To check the validity of the results of the hydrogen/oxygen propellant model velocity, temperature, and pressure were measured at the locations shown in Figure 7. Velocity was measured at the middle of the nozzle exit at (0,120,0) mm. Temperature and pressure were measured at the center of the mid-point of the combustion chamber at (0, -100,0) mm. These results were compared to experimental and numerical data from the works that boundary conditions were derived from [13-14]. The comparison of these results can be seen in Tables 4-5.

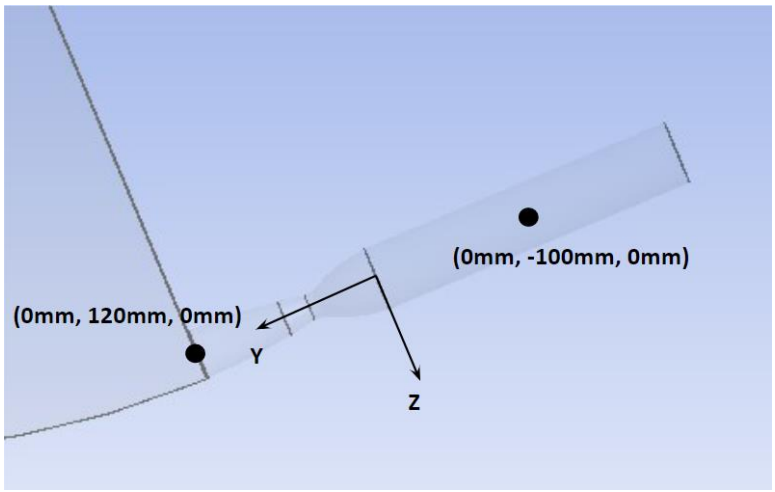

Figure 7. Position of Point Measurements.

Table 4. Data for Validation of Baseline Model [13-14].

Parameter	Numerical Comparison [14]	Experimental Comparison [13]
Velocity (m/s)	3900	Not Given
Temperature (K)	3354	3427
Pressure (MPa)	3.443	3.4

Table 5. Percent Error for Baseline Model.

Parameter	Hydrogen/Oxygen Baseline	% Error to Numerical	% Error to Experimental
Velocity (m/s)	3740	4.09%	N/A
Temperature (K)	3843	14.58%	12.14%
Pressure (MPa)	2.09	39.30%	38.53%

Out of the three parameters from the baseline compared to the work of Sullivan and Wang et al, velocity matched most closely: with a percent error of 4.09%. Results within a margin of 5% are typically considered to be acceptable when modeling. As a result, velocity measurements can be considered accurate in the case of the baseline and the methane/oxygen model which is based off it. Both temperature and pressure showed significant deviation, with pressure having the highest error at 39.30% and 38.53% when compared to the numerical and experimental results of Sullivan and Wang et al respectively. The cause of these errors is not precisely known but affects the validity of the model when considering these parameters. Consequently, attention should be paid to the apparent trends seen in temperature and pressure measurements rather than the exact numbers themselves.

II. Comparison of Results for Propellants

Point measurements were taken at the positions described previously in Figure 7 for both the hydrogen/oxygen and methane/oxygen propellant models, as seen in Table 6. As expected, the hydrogen/oxygen propellant had a higher exit velocity than the methane/oxygen propellant. This is because of the lighter nature of a molecule of hydrogen, which has less inertia compared to a molecule of methane, allowing more energy to be imparted to the exhaust of a hydrogen/oxygen propellant kinetically. A higher exit velocity directly correlates to a higher thrust, as mentioned previously (Eq. 3). The methane/oxygen propellant had a lower combustion chamber temperature, which was the opposite as was expected. The hydrogen/oxygen propellant also had a higher combustion chamber pressure. Both combustion chamber pressure and temperature directly contribute to nozzle exit velocity, with chamber pressure contributing the most, consequently hydrogen/oxygen propellant produces a higher thrust than methane/oxygen propellant.

Table 6. Point Measurements and Thrust for Models.

Model	**Velocity (m/s)**	**Temperature (K)**	**Pressure (MPa)**	**Calculated Thrust (N)**
Hydrogen/Oxygen	3740	3843	2.09	1162
Methane/Oxygen	2892	4742	1.32	898
% Difference	25.57%	20.94%	45.16%	25.63%

Nozzle exit velocity is also illustrated in Figures 8-9 as a line cross-section from the two walls of the nozzle exit. These figures illustrate the uniform nature of the flow exiting the rocket nozzles as well as the no-slip condition present at the nozzle walls. Throughout

the areas of the nozzles away from the walls, the velocity is nearly the same, with the hydrogen/oxygen propellant model appearing more uniform. The methane/oxygen propellant model is much less uniform, with its maximum velocity skewed to one side of the centerline of the nozzle, as seen in Figure 9. This is most likely a product of the model itself and may represent a need for further refinement of the mesh and/or model conditions. It could also represent flow separation on one side of the nozzle when using methane/oxygen, which could also explain the higher turbulence seen on the effected side of the nozzle in Figure 17.

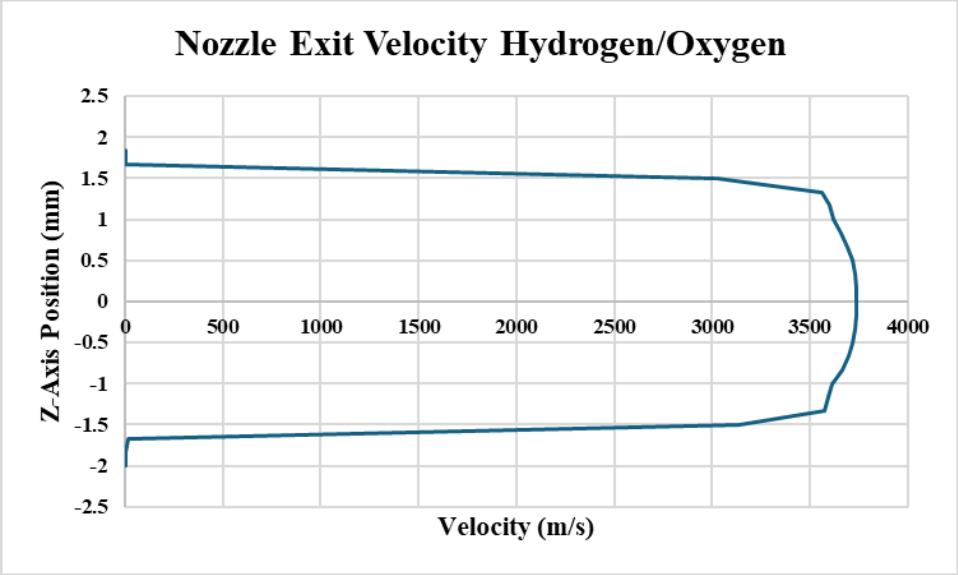

Figure 8. Hydrogen/Oxygen Nozzle Exit Velocity Cross-Section.

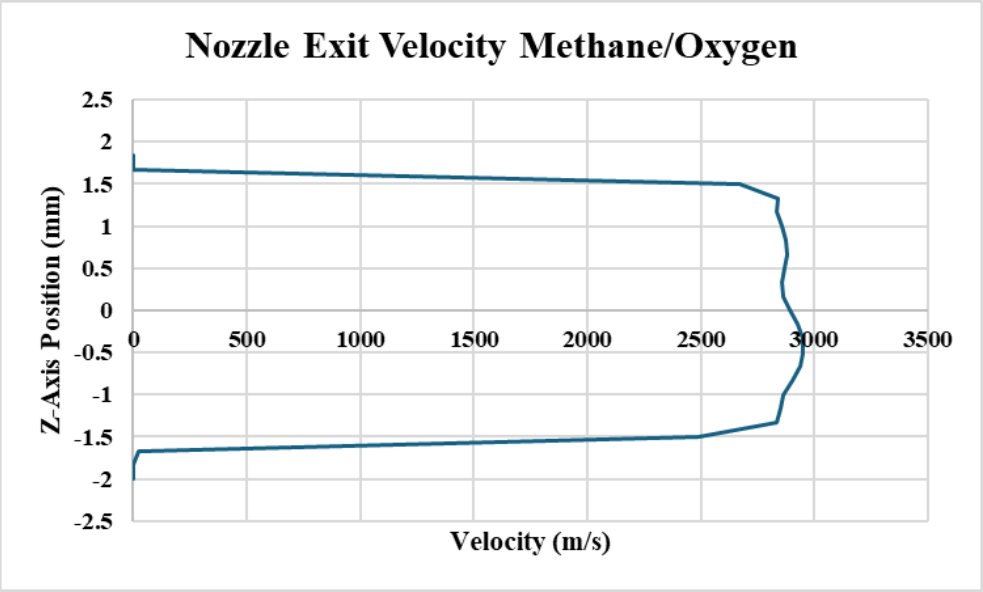

Figure 9. Methane/Oxygen Nozzle Exit Velocity Cross-Section.

The overall shape of the flow for each model matched well, along with velocity. The function of the aerospike is shown in Figures 10-13, where the flow, despite the low simulated atmospheric pressure of 11000 Pa remained relatively constrained for both the methane/oxygen and hydrogen/oxygen model. The methane/oxygen model experienced significant artifacting in the down-wind section from the nozzle exit. This led to the formation of a region with extremely exaggerated values for velocity, temperature, and TKE as seen in Figures 11, 13, and 17. Despite this, examination of the model found that this region did not affect the results in the areas of interest in the combustion chamber, nozzle, and aerospike. The cause of this problem is not understood but may be a result of meshing refinement.

The hydrogen/oxygen model experienced more fanning of its exhaust as seen in Figures 10-13 and 16-17 when compared to the methane/oxygen model. This is most obvious in the temperature contours where the exhaust of the hydrogen/oxygen model is significantly

more fanned out than that of the methane/oxygen model. The hydrogen/oxygen model also experienced a very abrupt fanning out, whereas the methane/oxygen model experienced a smoother, more gradual fanning out. This correlates with a higher magnitude and broader region of turbulence kinetic energy experienced by the hydrogen/oxygen model seen in Figures 16-17. The more directed exhaust of the methane/oxygen propellant could result in a less undirected array of thrust vectors compared to hydrogen/oxygen propellant.

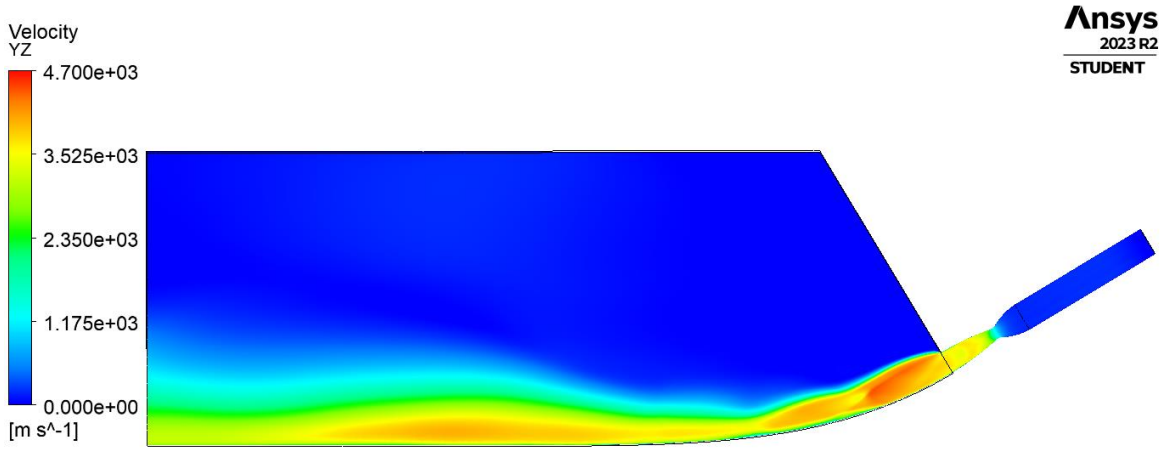

Figure 10. Hydrogen/Oxygen Propellant Velocity Contours.

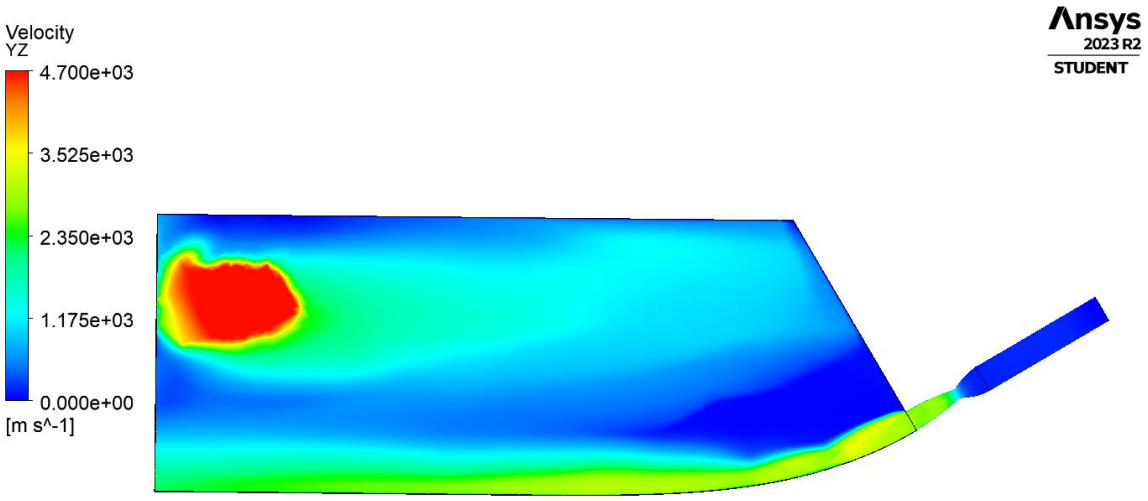

Figure 11. Methane/Oxygen Propellant Velocity Contours.

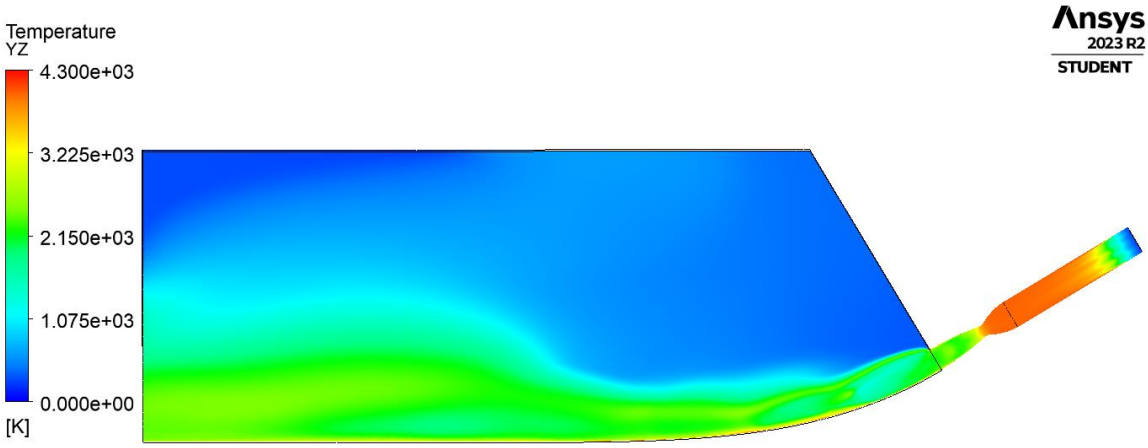

Figure 12. Hydrogen/Oxygen Propellant Temperature Contours.

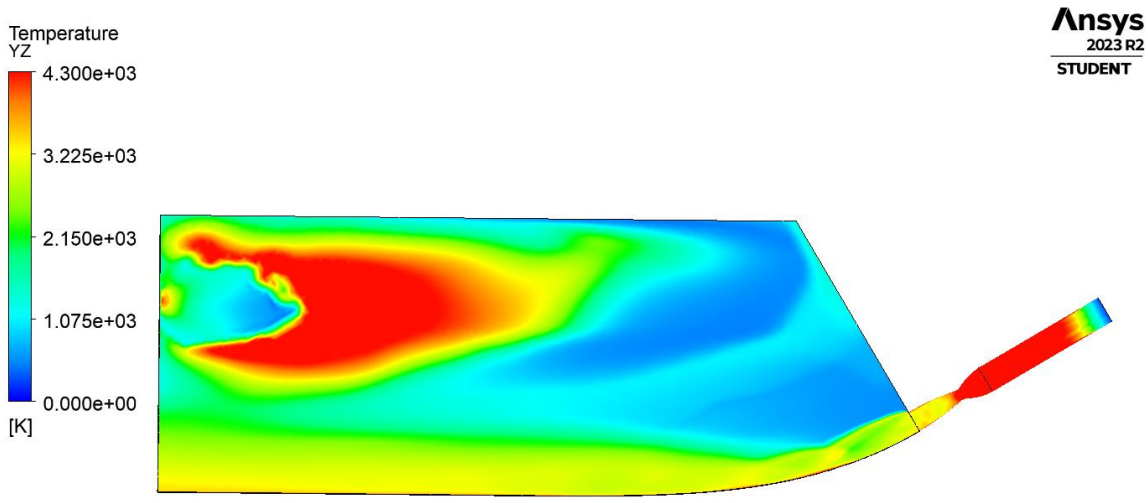

Figure 13. Methane/Oxygen Propellant Temperature Contours.

The contour diagrams for the pressure results of both models can be seen in Figures 14-15. Both models exhibited the expected behavior in terms of pressure. Pressure is essentially uniform in the combustion chamber of each model. This is as expected. Pressure then precipitously drops as potential and chemical energies are exchanged for kinetic energy. This occurs around the throat of the nozzle, as expected, as the flow cannot experience a velocity higher than Mach 1 until after surpassing the throat of the engine.

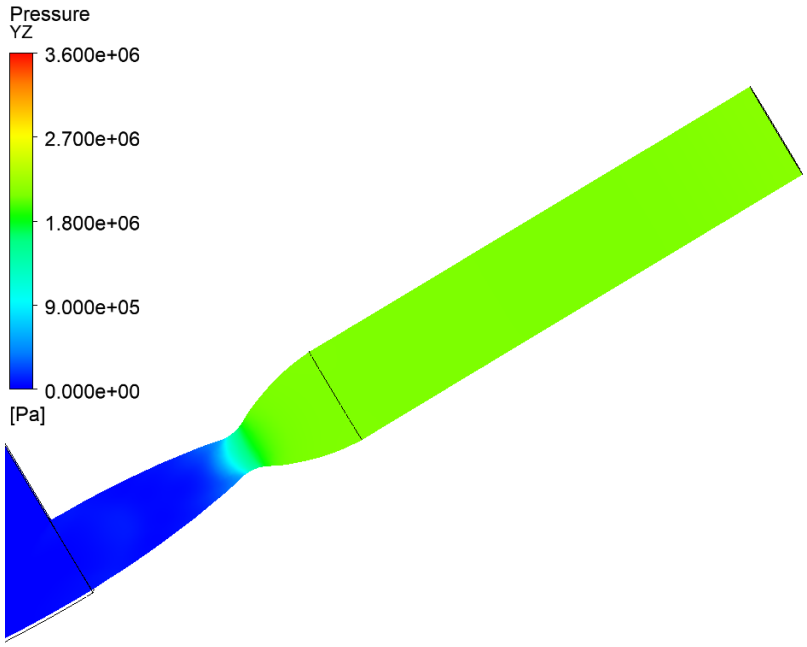

Figure 14. Hydrogen/Oxygen Propellant Pressure Contours.

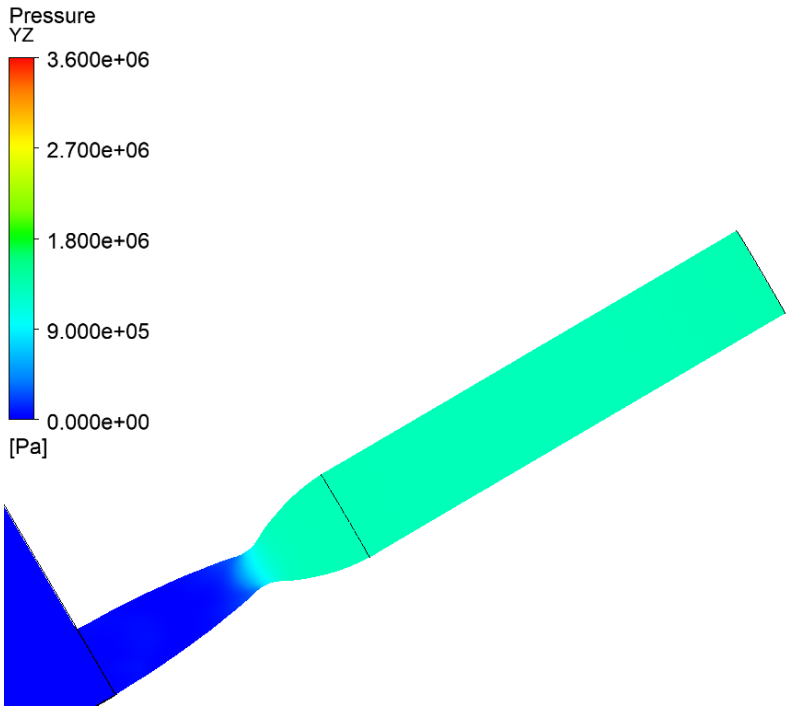

Figure 15. Methane/Oxygen Propellant Pressure Contours.

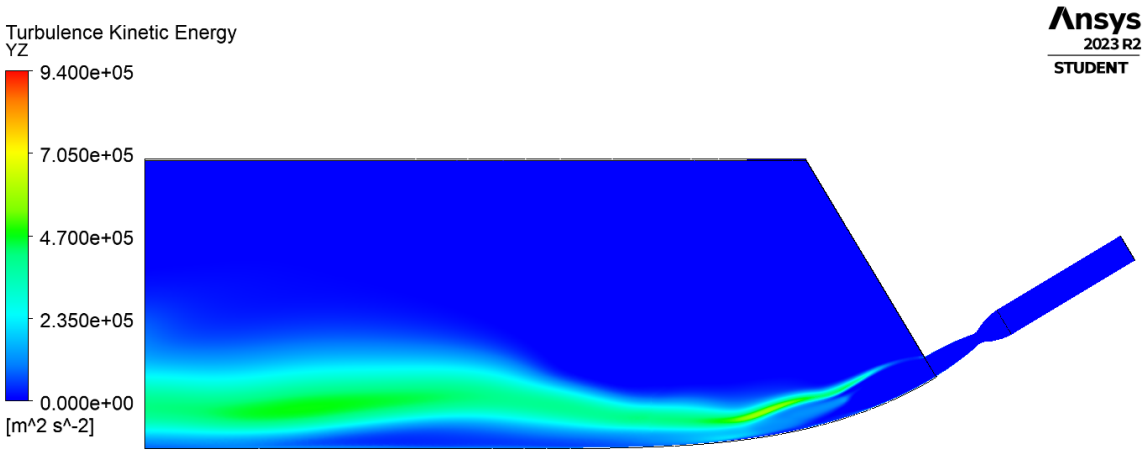

Figure 16. Hydrogen/Oxygen Propellant TKE Contours.

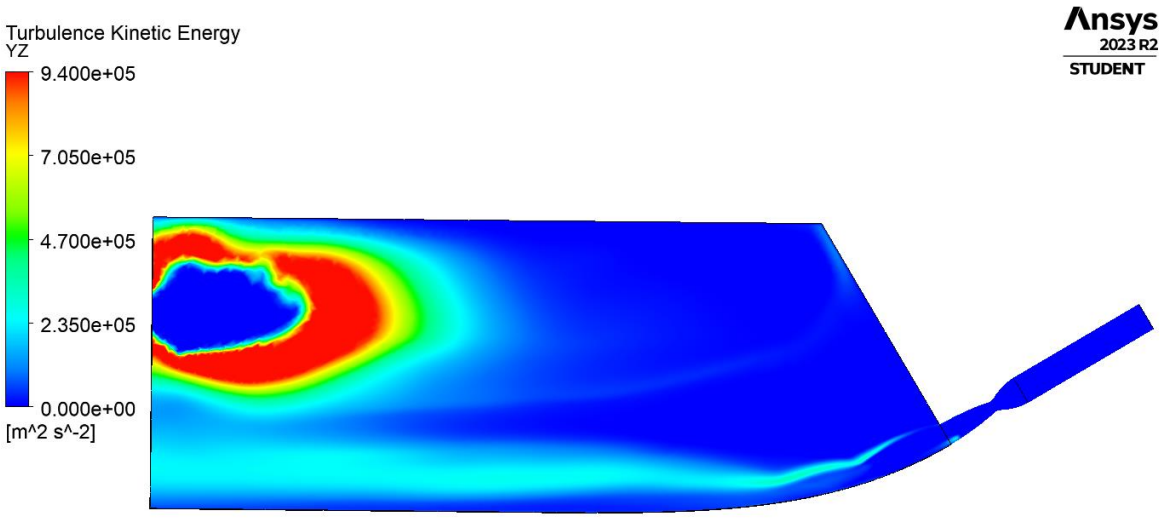

Figure 17. Methane/Oxygen Propellant TKE Contours.

Species contour diagrams were included for the propellant and exhaust species of each model in Figures 18-24. The contours, particularly those of the exhaust species also

illustrate the points that were discussed about flow shape earlier. Both models also had a significant amount of left of fuel, H_2 and CH_4, leftover in their exhausts. This is because both models were simulated with a fuel rich propellant mixture. Rocket engines always run fuel rich, as superheated oxidizers like oxygen tend to erode internal surfaces, shortening engine lifespan.

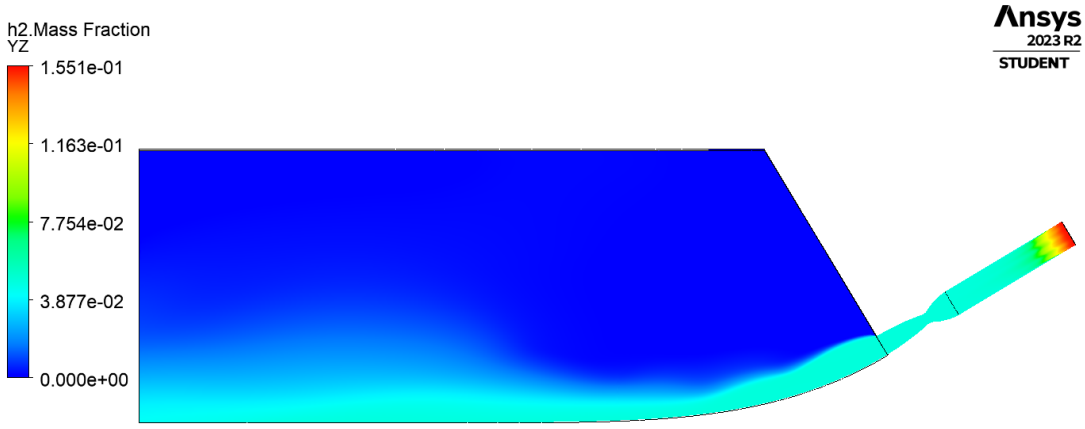

Figure 18. Hydrogen/Oxygen Propellant H_2 Mass Fraction Contours.

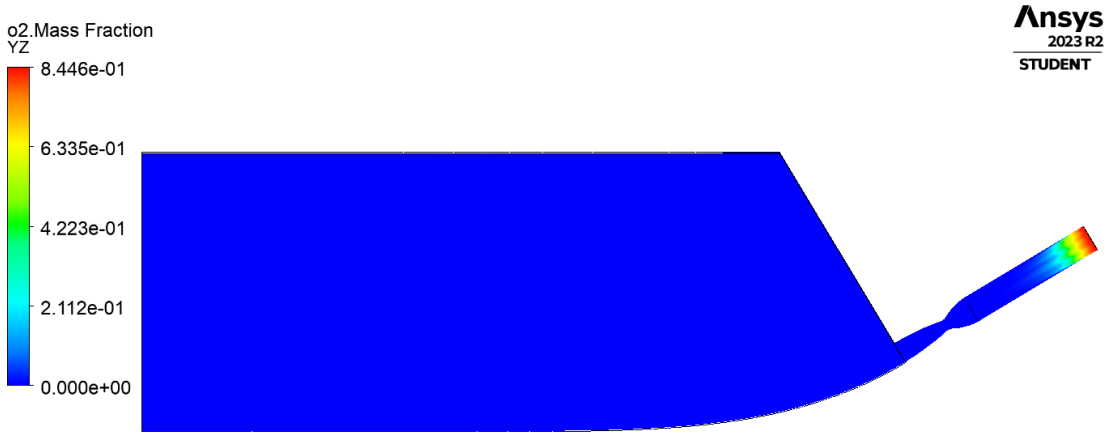

Figure 19. Hydrogen/Oxygen Propellant O_2 Mass Fraction Contours.

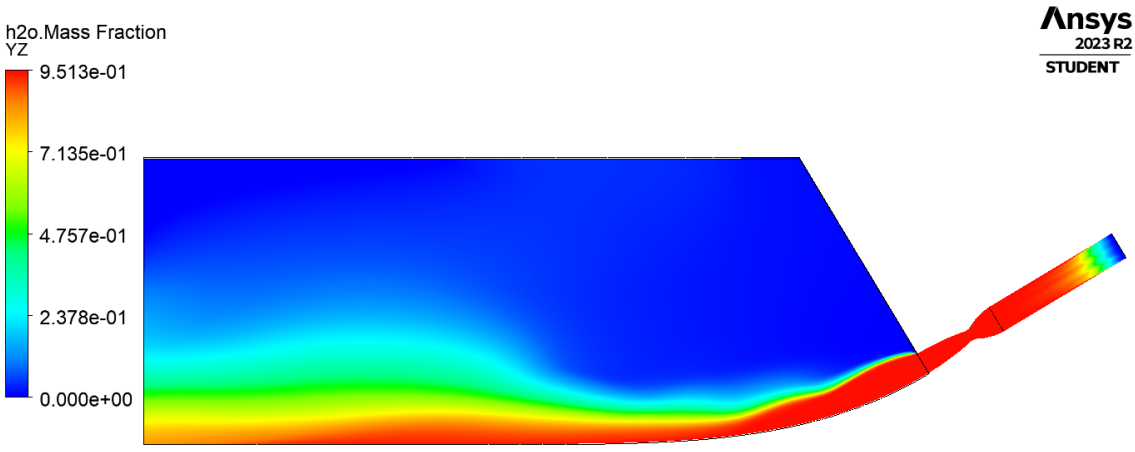

Figure 20. Hydrogen/Oxygen Propellant H_2O Mass Fraction Contours.

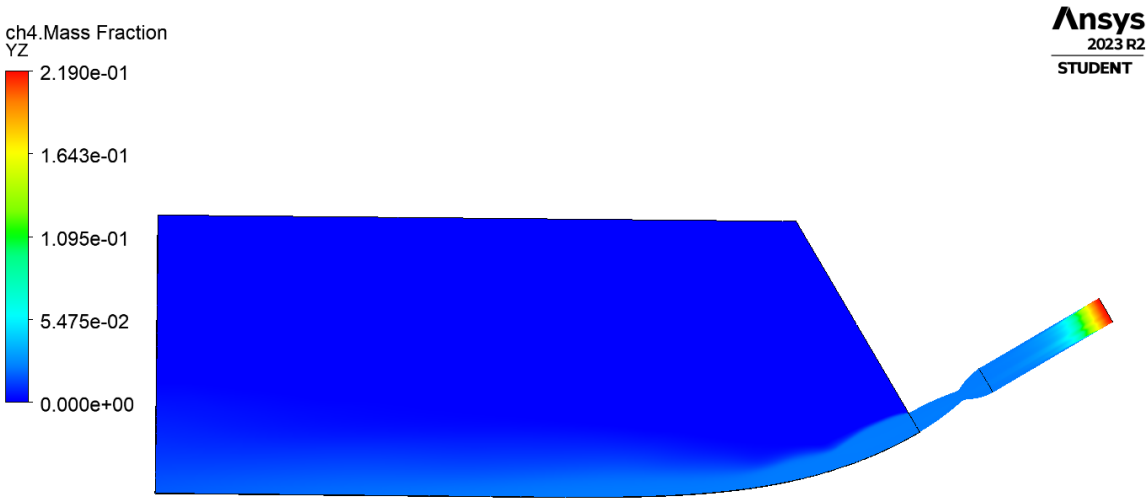

Figure 21. Methane/Oxygen Propellant CH_4 Mass Fraction Contours.

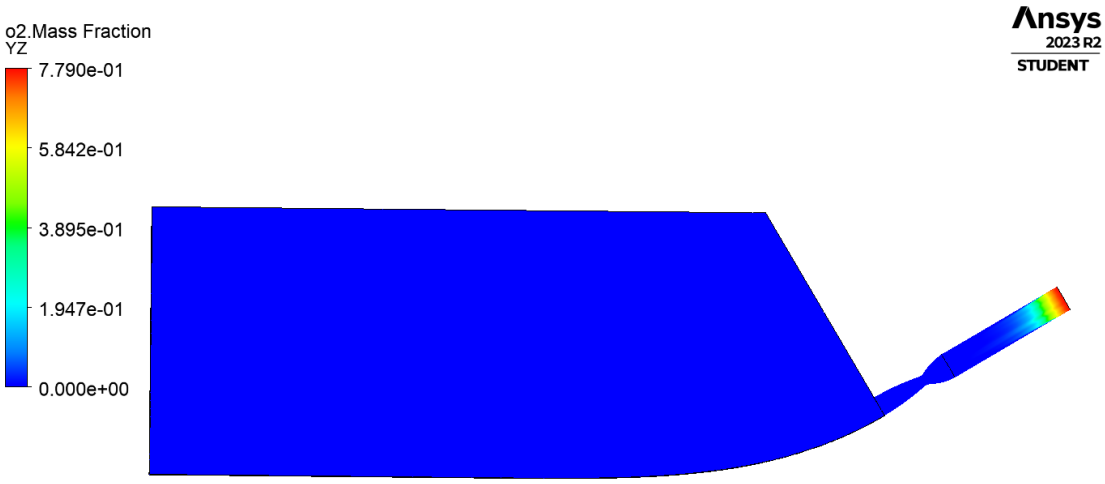

Figure 22. Methane/Oxygen Propellant O_2 Mass Fraction Contours.

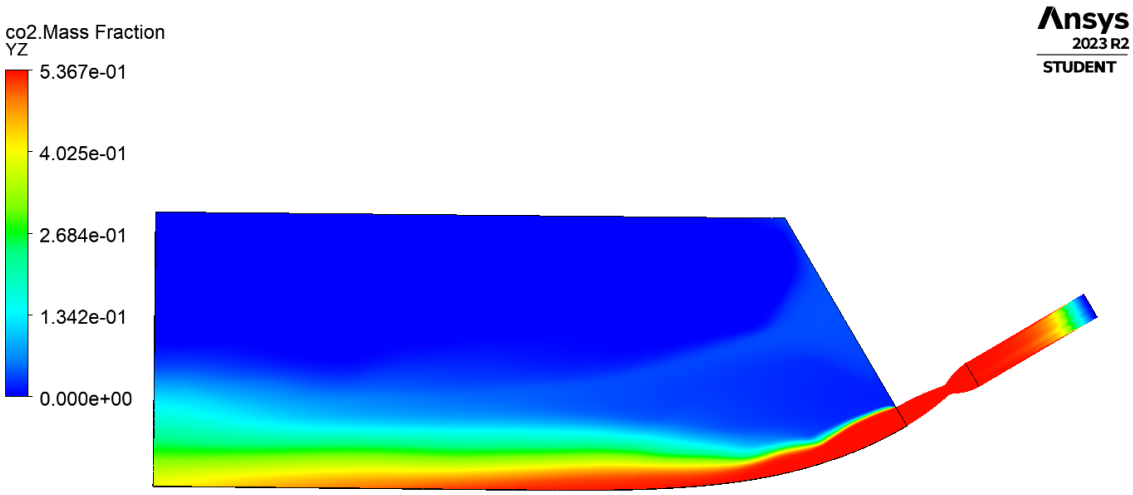

Figure 23. Methane/Oxygen Propellant CO_2 Mass Fraction Contours.

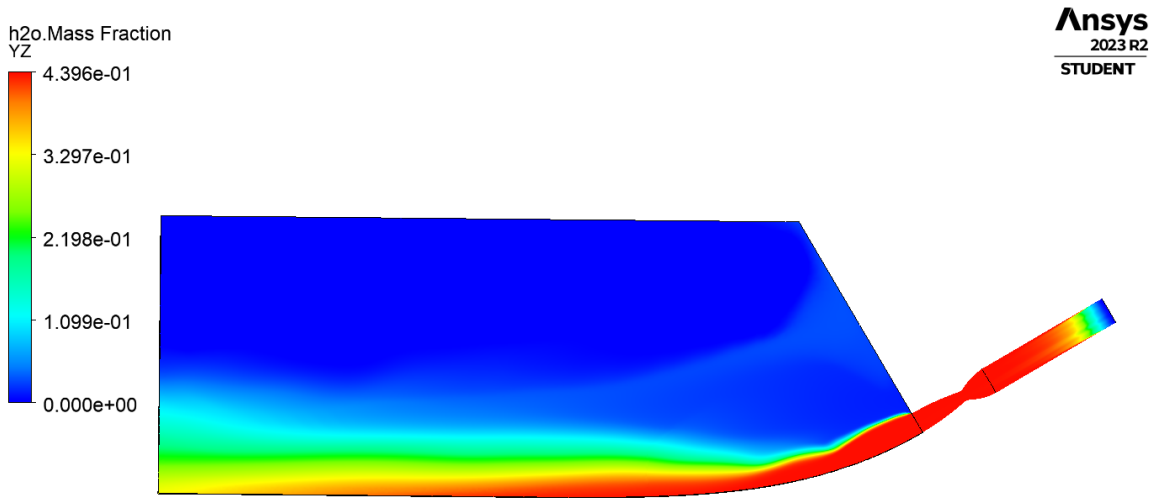

Figure 24. Methane/Oxygen Propellant H_2O Mass Fraction Contours.

Chapter 5: Conclusions

I. Conclusions

The results of this work showed varying degrees of success. A baseline was created using hydrogen/oxygen propellant to be compared to methane/oxygen propellant on a linear aerospike. Results for velocity matched well, with a percent error of 4.09%. As expected, the methane/oxygen model produced lower nozzle exit velocities than the hydrogen/oxygen model, likely due to the larger size of the methane molecule. Higher combustion temperatures were experienced by the methane/oxygen model, contrary to expectations. Significant differences in exhaust expansion were seen at the end of the aerospike for each model, with the methane/oxygen model experiencing less fanning out. Some issues were encountered when modeling methane/oxygen propellant that resulted in a large artifact within the domain, the cause of this is currently unclear. Despite this trends and values for results were reasonable.

II. Future Work

The current state of the methane/oxygen model leaves something to be desired. The first step to any future work is to investigate the cause of the artifact present in the model and remedy it. The values for temperature and pressure of the baseline hydrogen/oxygen model need to also be remedied.

One of the most interesting results found was the difference in fanning out of the exhausts of the different propellants. This likely has a direct effect on the efficiency of thrust generated and should be further studied at different altitudes. This would be interesting to pair with a study of the thrust produced per kilogram of fuel for each model.

One major problem common to larger aerospike engines is overheating of the spike. This can be addressed in several ways but should be explored and compared for different fuels. Future work could compare the cooling efficiency of methods like regenerative cooling for methane/hydrogen versus hydrogen/oxygen propellants.

References

[1] Jones, Harry. “The Recent Large Reduction in Space Launch Cost.” 48th International Conference on Environmental Systems, Albuquerque, NM, 8-12 July, 2018, ICES-2018-81. http://hdl.handle.net/2346/74082.

[2] Mark, Klem. “LOX/Methane In-Space Propulsion Systems Technology Status and Gaps.” NASA Report No. 20170005557, El Paso, TX, 2017.

[3] Zubrin, Robert and Muscatello, Anthony and Berggren, Mark. “Integrated Mars In Situ Propellant Production System.” *ASCE Journal of Aerospace Engineering* Vol. 26 Issue 1 (2013). 10.1061/ (ASCE)AS.1943-5525.0000201.

[4] Sutton, George and Biblarz, Oscar, *Rocket Propulsion Elements*. John Wiley and Sons, New Jersey (2017).

[5] Hagemann, Gerald and Immich, Hans and Nguyen, Thong Van and Dumnov, Gennady. “Advanced Rocket Nozzles.” *AIAA Journal of Propulsion and Power* Vol. 14 No.5 (1998). https://doi.org/10.2514/2.5354.

[6] Rao, Gadicharla. “Recent Development in Rocket Nozzle Configurations.” *AIAA Rocket Society Archive* Vol. 31 No. 11 (1961). https://doi.org/10.2514/8.5837.

[7] Craddock, C., Platt, D., 2019, “Aerospike Rocket Engine.” U.S. Patent US20200049103A1.

[8] Ehresman, C. “The Innovative Early Years of the General Electric Company’s Efforts in Rocket Propulsion Development.” *41st AIAA/ASME/SAE/ASEE Joint Propulsion Conference & Exhibit*: AIAA 2005-3536. Tucson, AZ, 10-13 July, 2005. https://doi.org/10.2514/6.2005-3536.

[9] Swet, C., J., 1961, “Plug nozzle rocket.” United States, US3358453.

[10] Rao, G.V.R, 1958, "Exhaust Nozzle Contour for Optimum Thrust," *AIAA Jet Propulsion Archive* Vol. 28 No. 6 (1958). https://doi.org/10.2514/8.7324.

[11] C., Lee. "FORTRAN Program for Plug Nozzle Design." NASA Report No. NASA CR-51300. NASA, Huntsville, AL. 1963.

[12] Angelino, Gianfranco. "Approximate Method for Plug Nozzle Design." *AIAA Journal* Vol. 2 No. 10 (1964): pp. 1834-1835. https://doi.org/10.2514/3.2682.

[13] Wang, Chang-Hui and Liu, Yu and Qin, Li-Zi. "Aerospike nozzle contour design and its performance validation." *Acta Astronautica* Vol. 64 (2009): pp. 1264-1275. https://doi.org/10.1016/j.actaastro.2008.01.045.

[14] Sullivan, Geoffrey. "CFD and Heat Transfer Analysis of Rocket Cooling Techniques on an Aerospike Nozzle." Masters Thesis 2465, Georgia Southern University, Statesboro, GA. 2022. https://digitalcommons.georgiasouthern.edu/etd/2465.

[15] Yang, Wei and Sun, Bing. "Numerical simulation of liquid film and regenerative cooling in a liquid rocket." *Applied Thermal Engineering* Vol. 54 (2013): pp. 460-469. https://doi.org/10.1016/j.applthermaleng.2013.02.021.

[16] Song, Jiawen and Sun, Bing. "Coupled numerical simulation of combustion and regenerative cooling in LOX/Methane rocket engines." *Applied Thermal Engineering* Vol. 106 (2016): pp. 762-773. https://doi.org/10.1016/j.applthermaleng.2016.05.130.

[17] 2013, *Ansys Fluent Theory Guide*, Release 15.0, ANSYS, Inc., Canonsburg, PA.

[18] Tenny, K. M., Cooper, J. S., 2022, "Ideal Gas Behavior." From https://europepmc.org/article/nbk/nbk441936#__NBK441936_dtls__.